2 ME338A - Homework

Due: Feb 04, 2010, 12pm

In spite of tremendous improvements during the past 20 years, heart failure remains one of the most common, costly, disabling, and deadly medical conditions affecting more than 25 million people worldwide. Despite the wide variety of pharmacological, surgical, device, and tissue engineered treatment strategies currently under investigation, patients with heart failure continue to experience progressive worsening of symptoms, frequent admission to the hospital, and premature death. Surgical strategies to reverse strain abnormalities in the ventricular wall are currently being recognized as a new paradigm for preventing the progression of heart failure. In an attempt to quantify strain profiles in the beating heart, researchers in the lab of Prof. D. Craig Miller in the Department of Cardiothoracic Surgery in the School of Medicine at Stanford have developed a novel technique to measure infarct-induced changes of ventricular wall kinematics in ovine models. They inserted two transmural beadsets, one in the anterior basal and one in the lateral lateral equatorial left ventricular wall, and silhouetted the left ventricular chamber with an additional thirteen subepicardial markers as illustrated in Figure 1. Videofluoroscopic images at 60 frames per second were acquired of all radiopaque markers using a biplane videofluoroscopy system with the heart in normal sinus rhythm and ventilation transiently arrested at end expiration. Marker coordinates from each of the biplane views were then merged to yield the 3D coordinates of each marker centroid in each frame using semi-automated image processing and digitization software. To determine local muscle fiber directions, transmural rectangular blocks of myocardial tissue were removed directly contiguous and basal to the implanted marker columns. Each block was sliced into 1mm thick transmural sections. For each section, fiber angles were measured between the local cardiomyocyte axis and the global circumferential axis. **The objective of this homework is to quantify ventricular wall strains and characterize muscle fiber contraction in the beating heart.** This homework can help to answer the following scientific and clinical questions: Does fiber contraction display regional and transmural variations? How do contraction profiles change with infarction? Can these changes be prevented through passive support? Is the fiber contraction of the non-infarcted myocardium inherently normal? Does the failing heart dilate uniformly or is dilation distributed heterogeneously?

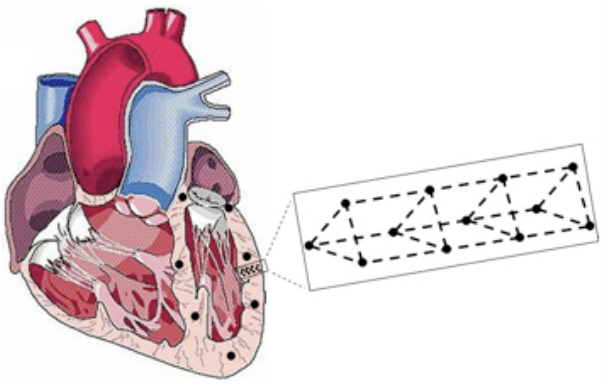

Fig. 1 Heart with ventricular markers and beadset

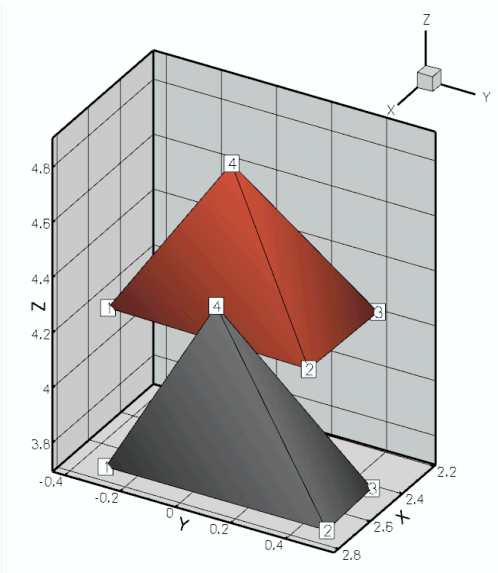

Fig. 2 Coordinates of ventricular beadset

Figure 2 shows a typical data set of four markers of the beadset array. The grey tetrahedron shows the marker positions $\boldsymbol{X}$ at end diastole, i.e., at the end of the cardiac filling phase. The red tetrahedron illustrates the marker positions $\boldsymbol{x}$ at end systole, i.e., at the end of the cardiac contraction phase. You can assume that the tetrahedron in Figure 2 is oriented such that its $\boldsymbol{e}_3$ (or $\boldsymbol{z}$) axis is aligned with in the longitudinal direction of the heart, and that $\boldsymbol{e}_1$ (or $\boldsymbol{x}$) and $\boldsymbol{e}_2$ (or $\boldsymbol{y}$) are the radial/transmural and circumferential directions, respectively. Just to give you an idea, the left ventricular chamber is about 8 cm long and has a maximum radius of approximately 4 cm. The measured marker coordinates are given below.

$$\boldsymbol{X}_1 = [\ +2.80\ \ -0.27\ \ +3.75\ ]^t \qquad \boldsymbol{x}_1 = [\ +2.56\ \ -0.40\ \ +4.17\ ]^t$$
$$\boldsymbol{X}_2 = [\ +2.80\ \ +0.53\ \ +3.75\ ]^t \qquad \boldsymbol{x}_2 = [\ +2.55\ \ +0.32\ \ +4.15\ ]^t$$
$$\boldsymbol{X}_3 = [\ +2.50\ \ +0.52\ \ +3.75\ ]^t \qquad \boldsymbol{x}_3 = [\ +2.22\ \ +0.38\ \ +4.21\ ]^t$$
$$\boldsymbol{X}_4 = [\ +2.80\ \ +0.13\ \ +4.45\ ]^t \qquad \boldsymbol{x}_4 = [\ +2.60\ \ +0.07\ \ +4.85\ ]^t$$

The histologically measured fiber orientation angle for the displayed tetrahedron, measured clockwise from the y-axis, is 45.4°. For the sake of simplicity, you can assume that the muscle fibers are planar in the transmural plane. Therefore, the cardiac muscle fiber direction $\boldsymbol{N}^{\text{fib}}$ in the relaxed diastolic configuration can thus be expressed through the following unit vector.

$$\boldsymbol{N}^{\text{fib}} = [\,0.0\ \ -\cos(\alpha)\ \ +\sin(\alpha)\,]^t \qquad \text{with} \qquad \alpha = 45.4^\circ$$

The overall objective is this homework is to determine the muscle fiber contraction during systole. This is pretty straightforward if you solve the following substeps!

[1] Determine three vectors $\mathrm{d}\boldsymbol{X}_i$ that span the tetrahedron at end diastole.
Take an arbitrary point of the tetrahedron as origin, e.g., $\boldsymbol{X}_1$, and calculate the three vectors $\mathrm{d}\boldsymbol{X}_2$, $\mathrm{d}\boldsymbol{X}_3$, and $\mathrm{d}\boldsymbol{X}_4$ from the origin to any other point using the coordinates $\boldsymbol{X}$ at end diastole such that $\mathrm{d}\boldsymbol{X}_i = \boldsymbol{X}_i - \boldsymbol{X}_1$ for $i = 2, 3, 4$.

[2] Determine the same three vectors $\mathrm{d}\boldsymbol{x}_i$ that span the tetrahedron at end systole.
Take the same point as origin, e.g., $\boldsymbol{x}_1$, and calculate the vectors $\mathrm{d}\boldsymbol{x}_2$, $\mathrm{d}\boldsymbol{x}_3$, and $\mathrm{d}\boldsymbol{x}_4$ from the origin to any other point using the coordinates $\boldsymbol{x}$ at end systole such that $\mathrm{d}\boldsymbol{x}_i = \boldsymbol{x}_i - \boldsymbol{x}_1$ for $i = 2, 3, 4$.

[3] Determine the deformation gradient tensor $\boldsymbol{F}$ that maps all diastolic line elements as $\mathrm{d}\boldsymbol{X}_i$ onto the systolic line elements $\mathrm{d}\boldsymbol{x}_i$.
$\boldsymbol{F} = \partial\boldsymbol{x} \,/\, \partial\boldsymbol{X}$ is called the deformation gradient and it is the key kinematic quantity to

characterize finite strain kinematics. It maps line elements according to $\mathrm{d}\boldsymbol{x}_i = \boldsymbol{F} \cdot \mathrm{d}\boldsymbol{X}_i$. Applying this mapping to all three line elements $\mathrm{d}\boldsymbol{X}_i$ defines three vector valued equations, i.e., nine equations to solve for the nine components of $\boldsymbol{F}$. To obtain a more compact notation, rearrange all diastolic line elements from [1] and all systolic line elements from [2] in 3×3 matrices $\boldsymbol{C} := [\ \mathrm{d}\boldsymbol{X}_1;\ \mathrm{d}\boldsymbol{X}_2;\ \mathrm{d}\boldsymbol{X}_3\ ]$ and $\boldsymbol{c} := [\ \mathrm{d}\boldsymbol{x}_1;\ \mathrm{d}\boldsymbol{x}_2;\ \mathrm{d}\boldsymbol{x}_3\ ]$. Now, determine the deformation gradient $\boldsymbol{F}$ and its inverse $\boldsymbol{F}^{-1}$ by solving the equations $\boldsymbol{F} \cdot \boldsymbol{C} = \boldsymbol{c}$ and $\boldsymbol{F}^{-1} \cdot \boldsymbol{c} = \boldsymbol{C}$, respectively. Verify your results by evaluating $\mathrm{d}\boldsymbol{x}_i = \boldsymbol{F} \cdot \mathrm{d}\boldsymbol{X}_i$ and $\mathrm{d}\boldsymbol{X}_i = \boldsymbol{F}^{-1} \cdot \mathrm{d}\boldsymbol{x}_i$ through the calculated deformation gradient and its inverse.

[4] Determine the systolic fiber direction $\boldsymbol{n}^{\text{fib}} = \boldsymbol{F} \cdot \boldsymbol{N}^{\text{fib}}$ and its normalized form $\bar{\boldsymbol{n}}^{\text{fib}}$ through $\bar{\boldsymbol{n}}^{\text{fib}} := \boldsymbol{n}^{\text{fib}} / \sqrt{\boldsymbol{n}^{\text{fib}} \cdot \boldsymbol{n}^{\text{fib}}}$
The deformation gradient can be used to map the measured diastolic fiber direction $\boldsymbol{N}^{\text{fib}}$ onto the systolic fiber direction $\boldsymbol{n}^{\text{fib}}$. Comment on how $\boldsymbol{N}^{\text{fib}}$ and $\boldsymbol{n}^{\text{fib}}$ deviate.

[5] Determine the fiber stretch $\lambda = \sqrt{\boldsymbol{n}^{\text{fib}} \cdot \boldsymbol{n}^{\text{fib}}}$.
Since the fiber orientation $\boldsymbol{N}^{\text{fib}}$ was given as a unit vector, the length of the systolic vector $\boldsymbol{n}^{\text{fib}} = \boldsymbol{F} \cdot \boldsymbol{N}^{\text{fib}}$ corresponds to the relative change in fiber length, i.e., the fiber stretch in the finite strain setting, $\lambda = \sqrt{\boldsymbol{n}^{\text{fib}} \cdot \boldsymbol{n}^{\text{fib}}} = \sqrt{\boldsymbol{N}^{\text{fib}} \cdot \boldsymbol{F}^{\text{t}} \cdot \boldsymbol{F} \cdot \boldsymbol{N}^{\text{fib}}}$.

[6] Determine the Green-Lagrange strain tensor $\boldsymbol{E} := \frac{1}{2}\left[\ \boldsymbol{F}^{\text{t}} \cdot \boldsymbol{F} - \boldsymbol{I}\ \right]$
The Green-Lagrange strain tensor $\boldsymbol{E}$ is used to characterize strains in the undeformed configuration in the finite strain setting.

[7] Determine the Euler-Almansi strain tensor $\boldsymbol{e} := \frac{1}{2}\left[\ \boldsymbol{I} - \boldsymbol{F}^{-\text{t}} \cdot \boldsymbol{F}^{-1}\ \right]$
The Euler-Almansi strain tensor $\boldsymbol{e}$ is used to measure strains in the deformed configuration in the finite strain setting.

[8] Determine the displacement gradient tensor $\boldsymbol{H} = \boldsymbol{F} - \boldsymbol{I}$.
$\boldsymbol{H} = \nabla \boldsymbol{u}$ is the nonsymmetric displacement gradient tensor which can also be expressed as $\boldsymbol{H} = \partial \boldsymbol{u} \,/\, \partial \boldsymbol{X} = \partial[\boldsymbol{x} - \boldsymbol{X}] \,/\, \partial \boldsymbol{X} = \boldsymbol{F} - \boldsymbol{I}$.

[9] Linearize the Green-Lagrange strain tensor $\boldsymbol{E}$ with the help of the Gateaux derivative to obtain the small strain tensor $\boldsymbol{\epsilon} = \frac{1}{2}\,(\boldsymbol{H} + \boldsymbol{H}^{\text{t}})$.
Linearize $\boldsymbol{E}$ formally, then calculate $\boldsymbol{\epsilon}$, compare the small strain approximation $\boldsymbol{\epsilon}$ with the large strain Green-Lagrange tensor $\boldsymbol{E}$, and comment on your results.

[10] Linearize the Euler-Almansi strain tensor $\boldsymbol{e}$ with the help of the Gateaux derivative to obtain the small strain tensor $\boldsymbol{\epsilon} = \frac{1}{2}\,(\boldsymbol{H} + \boldsymbol{H}^{\text{t}})$.
Linearize $\boldsymbol{e}$ formally to obtain $\boldsymbol{\epsilon}$, compare the small strain approximation $\boldsymbol{\epsilon}$ with the large strain Euler-Almansi tensor $\boldsymbol{e}$, and comment on your results.

[11] Determine the strain in the fiber direction by using different strain measures; that is, $\epsilon_n = \boldsymbol{N}^{\text{fib}} \cdot \boldsymbol{\epsilon} \cdot \boldsymbol{N}^{\text{fib}}$, $\epsilon_{nG} = \boldsymbol{N}^{\text{fib}} \cdot \boldsymbol{E} \cdot \boldsymbol{N}^{\text{fib}}$, $\epsilon_{nA} = \bar{\boldsymbol{n}}^{\text{fib}} \cdot \boldsymbol{e} \cdot \bar{\boldsymbol{n}}^{\text{fib}}$.
Compare the Green strain ϵ_{nG} and the Almansi strain ϵ_{nA} with the small strain approximation of the fiber contraction ϵ_n. Comment on your results. Do you think they are reasonable? Find evidence in the literature about the amount of maximum cardiomyocyte contraction.

[12] Let $\mathrm{d}V$ and $\mathrm{d}v$ denote the volume of the tetrahedron at end diastole and end systole, respectively. Show that these volumes are related through the volume map $\mathrm{d}v = J\mathrm{d}V$ where J is the Jacobian $J := \det(\boldsymbol{F})$.
You might find it useful to take the definition of the determinant through the scalar triple vector product as a departure point. Recall that the scalar triple vector product corresponds to the volume of the parallelepiped spanned by the three vectors.

[13] Linearize the non-linear measure of dilation $\mathcal{E} := (\mathrm{d}v - \mathrm{d}V)/\mathrm{d}V = (J-1)$ to obtain the linearized dilation $e = \mathrm{tr}(\boldsymbol{\epsilon})$.
Comment on whether the tissue behaves compressible or incompressible and on whether this was what you would have expected.

You can use MATLAB to solve the matrix and vector operations. If you choose to do so, you must deliver a printout of your MATLAB code with the homework.

Additional reading Cheng A, Nguyen T, Malinowski M, Daughters GT, Miller DC, Ingels NB. Heterogeneity of left ventricular wall thickening mechanisms. Circulation, 2008;118:713-721.

Heterogeneity of Left Ventricular Wall Thickening Mechanisms

Allen Cheng, MD; Tom C. Nguyen, MD; Marcin Malinowski, MD; George T. Daughters, MS; D. Craig Miller, MD; Neil B. Ingels, Jr, PhD

Background—Myocardial fibers are grouped into lamina (or sheets) 3 to 4 cells thick. Fiber shortening produces systolic left ventricular (LV) wall thickening primarily by laminar extension, thickening, and shear, but the regional variability and transmural distribution of these 3 mechanisms are incompletely understood.

Methods and Results—Nine sheep had transmural radiopaque markers inserted into the anterior basal and lateral equatorial LV. Four-dimensional marker dynamics were studied with biplane videofluoroscopy to measure circumferential, longitudinal, and radial systolic strains in the epicardium, midwall, and endocardium. Fiber and sheet angles from quantitative histology allowed transformation of these strains into transmural contributions of sheet extension, thickening, and shear to systolic wall thickening. At all depths, systolic wall thickening in the anterior basal region was 1.6 to 1.9 times that in the lateral equatorial region. Interestingly, however, systolic fiber shortening was identical at each transmural depth in these regions. Endocardial anterior basal sheet thickening was >2 times greater than in the lateral equatorial region (epicardium, 0.16±0.15 versus 0.03±0.06; endocardium, 0.45±0.40 versus 0.17±0.09). Midwall sheet extension was >2 times that in the lateral wall (0.22±0.12 versus 0.09±0.06). Epicardial and midwall sheet shears in the anterior wall were ≈2 times higher than in the lateral wall (epicardium, 0.14±0.07 versus 0.05±0.03; midwall, 0.21±0.12 versus 0.12±0.06).

Conclusions—These data demonstrate fundamentally different regional contributions of laminar mechanisms for amplifying fiber shortening to systolic wall thickening. Systolic fiber shortening was identical at each transmural depth in both the anterior and lateral LV sites. However, systolic wall thickening of the anterior site was much greater than that of the lateral site. Fiber shortening drives systolic wall thickening, but sheet dynamics and orientations are of great importance to systolic wall thickening. LV wall thickening and its clinical implications pivot on different wall thickening mechanisms in various LV regions. Attempts to implant healthy contractile cells into diseased hearts or to surgically manipulate LV geometry need to take into account not only cardiomyocyte contraction but also transmural LV intercellular architecture and geometry. **(*Circulation*. 2008;118:000-000.)**

Key Words: myocardial contraction ■ fibers and sheets ■ strain ■ wall thickening ■ ventricles ■ systole ■ mechanics

Left ventricular (LV) wall thickening is a significant contributor to stroke volume. Although myocardial fiber contraction provides the cellular basis for regional myocardial wall thickening, 15% fiber shortening leads to only an 8% increase in myocyte diameter, which cannot explain the observed >40% radial LV wall thickening and >60% ejection fraction.[1,2] Myocardial fibers have been shown to be grouped into laminar "sheets" 3 to 4 cells thick that are interconnected by an extensive extracellular matrix.[3,4] Spotnitz et al[5] first suggested that reorientation of transmural sheets of fibers could provide a basis for wall thickness changes. LeGrice et al[3,4] showed that longitudinal-radial shear of these sheets was likely to be an important mechanism underlying systolic wall thickening. Costa et al[1] extended this work, showing that systolic sheet extension and sheet-normal shear were the primary determinants of systolic wall thickening. Despite these important findings, the regional distribution and mechanisms of systolic wall thickening within the LV myocardium remain poorly understood. The objective of this study was to examine the regional variability and transmural distribution of fiber-sheet strains and their contribution to systolic wall thickening.

Received October 9, 2007; accepted June 6, 2008.

From the Department of Cardiovascular and Thoracic Surgery, Stanford University School of Medicine, Stanford (A.C., T.C.N., M.M., G.T.D., D.C.M., N.B.I.), and the Laboratory of Cardiovascular Physiology and Biophysics, Research Institute of the Palo Alto Medical Foundation, Palo Alto (G.T.D., N.B.I.), Calif.

Presented in part at the 2005 American Heart Association Scientific Sessions, Dallas, Tex, November 15, 2005, and published in abstract form (*Circulation*. 2005;112[suppl II]:II-618).

The online Data Supplement can be found with this article at http://circ.ahajournals.org/cgi/content/full/CIRCULATIONAHA.107.744623/DC1.

Correspondence to Neil B. Ingels, Jr, PhD, Laboratory of Cardiovascular Physiology and Biophysics, Research Institute, Palo Alto Medical Foundation, 795 El Camino Real (Ames Bldg), Palo Alto, CA 94301. E-mail ingels@stanford.edu

© 2008 American Heart Association, Inc.

Circulation **is available at http://circ.ahajournals.org** **DOI: 10.1161/CIRCULATIONAHA.107.744623**

Downloaded from circ.ahajournals.org at STANFORD UNIV MEDICAL CENTER on January 27, 2010

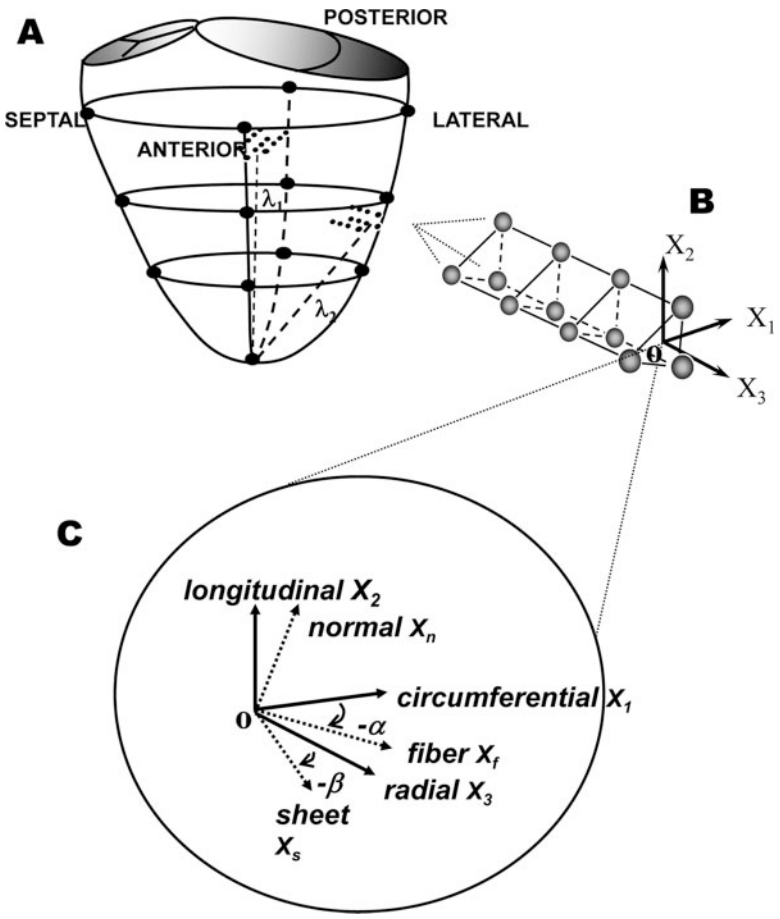

Figure 1. A, Locations of LV epicardial markers (large filled circles) and LV lateral equatorial and anterior basal transmural bead sets (small filled circles). B, Transmural tissue blocks for histological measurements were excised from each heart at the anterior basal and lateral equatorial regions immediately below the transmural bead sets, with the edges cut parallel to X_1, X_2, and X_3, the circumferential, longitudinal, and radial cardiac axes, respectively. C, Transmural α was measured from sections cut parallel to the X_1–X_2 plane. At a given wall depth, measured α and β were used to define local fiber-sheet coordinates with basis vectors of fiber axis (X_f), sheet axis perpendicular to X_f within sheet plane (X_s), and axis normal to the sheet plane (X_n). These same measurements were obtained from the anterior wall tissue block.

Editorial p ●●●
Clinical Perspective p ●●●

Methods

All animals received humane care in compliance with the *Principles of Laboratory Animal Care* formulated by the National Society for Medical Research and the *Guide for Care and Use of Laboratory Animals* prepared by the National Academy of Sciences and published by the National Institutes of Health (DHEW NIHG publication 85-23, revised 1985). This study was approved by the Stanford Medical Center Laboratory Research Animal Review Committee and was conducted according to Stanford University policy. The surgical preparation and marker data acquisition methods have been described in detail previously.[6–10]

Surgical Preparation

Nine adult Dorsett-hybrid sheep (McGrew Farm, Calif) were premedicated with ketamine (25 mg/kg IM), intubated, and ventilated. Anesthesia was maintained with inhalation isoflurane (1% to 2.5%). The heart was exposed through a left thoracotomy, and 13 subepicardial helical tantalum radiopaque markers were surgically implanted to silhouette the LV chamber (Figure 1A). Epicardial echocardiography was used to identify a segment of the midlateral equatorial LV wall between the papillary muscles and in the anterior LV wall basal to the anterior papillary muscle. After the measurement of wall depth of these 2 regions, 3 transmural columns of beads (three 0.7-mm-diameter gold beads implanted from the endocardium to epicardium and one 1.7-mm bead sewn onto the epicardial surface above each column; Figure 1B) were then implanted into these 2 segments using a bead insertion trocar oriented normal to the regional epicardial tangent plane.

Data Acquisition

Immediately after the operation, the animals were taken to the catheterization laboratory. Each animal was placed in the right lateral decubitus position and kept ventilated, and anesthesia was maintained with inhalation isoflurane (1% to 2.5%). A micromanometer-tipped catheter (model MPC-500, Millar Instruments, Houston, Tex) calibrated in a 37°C water bath was inserted into the LV via a carotid artery catheter. Philips Optimus 2000 biplane Lateral ARC 2/Poly DIAGNOST C2 system (Philips Medical Systems, North America Co, Pleasanton, Calif) was used to acquire biplane videofluoroscopic (60-Hz) images of all radiopaque markers and bead sets. Two-dimensional images from 2 radiographic views were digitized and merged to yield 3-dimensional coordinates for each marker and bead for every frame (ie, every 16.7 ms). Simultaneous biplane videofluoroscopy, LV pressure, aortic pressure, and ECG signal were recorded in the steady-state, baseline open-chest condition with the heart in sinus rhythm and ventilation briefly arrested at end expiration.

Three consecutive steady-state beats in sinus rhythm were selected for analysis from each study. For each cardiac cycle, end diastole was defined as the videofluoroscopic frame immediately before the upstroke of the LV pressure curve, defined by dLVP/dt $>$120 mm Hg/s. End systole was defined as the videofluoroscopic frame when d^2LVP/dt^2 changed from sing from minus to plus, a definition that captures the onset of relaxation.

After the study, conventional 3.0-mm perfusion balloon catheters (GUIDANT AguilTrac Peripheral Catheter, Santa Clara, Calif) were advanced in the proximal left anterior descending and circumflex arteries. An intravenous bolus of sodium pentothal (1 g IV) was given, and the heart was arrested at end diastole with an intravenous potassium chloride bolus (80 mEq). LV pressure was adjusted by blood withdrawal to match the previous in vivo LV end-diastolic pressure, defined as the pressure immediately preceding the upstroke of the LV pressure curve in the beating heart. To fix the heart in situ,

Downloaded from circ.ahajournals.org at STANFORD UNIV MEDICAL CENTER on January 27, 2010

Table 1. Transmural Fiber and Sheet Angles

	Fiber Angle, α, Degrees			Sheet Angle, β, Degrees		
	Subepicardium	Midwall	Subendocardium	Subepicardium	Midwall	Subendocardium
Anterobasal wall	−37±6	−8±7	24±11	−55±10	43±5	−52±10
Lateral equatorial wall	−37±8	−8±9	21±10	46±7	−37±4	53±8

Group mean±SD data from 9 hearts. See text and Figure 1 for details about fiber and sheet angles.

300 mL buffered glutaraldehyde (5%) was infused simultaneously into both the anterior descending and left circumflex coronary arteries. The heart was then explanted and stored in 10% formalin for later fiber and sheet angle and wall thickness examination.

Histological Measurements

A transmural rectangular block of myocardial tissue, directly contiguous and basal to the implanted marker columns (Figure 1B), was removed from the ventricular wall from both the anterior basal and lateral equatorial regions, with the edges of the block cut parallel to the local circumferential (X_1), longitudinal (X_2), and radial (X_3), (Figure 1B) axes of the left ventricle. Each block was sliced into sequential 1-mm–thick sections parallel to the X_1–X_2 plane, thereby providing a series of slices from the epicardium to endocardium for measurement of fiber angle (α). The fiber angle, defined as the angle between the local muscle fiber axis (X_f) and circumferential axis (X_1; Figure 1C), was measured at 5 sites on each image with image processing software (SPOT Advanced Version 4.0.1, Diagnostic Instruments, Inc, Sterling Heights, Mich). Mean α was used to characterize the fiber angle at each transmural depth. Two parallel cuts separated by ≈1 mm were then made normal to the fiber axis in each of these transmural sections. The samples were kept moist with a 30% sucrose solution to avoid the distortional effects of dehydration and to minimize freezing artifact during direct histological measurements of sheet angle (β) from the sheet-normal plane. The fiber-normal slices were placed in 15×15×5-mm plastic molds (Tissue-Tek, Cryomold Intermediate, Miles Inc, Elkhart, Ind), embedded in optical coherence tomography compound (Tissue-Tek, Sakura Finetek USA Inc, Torrance, Calif), frozen over dry ice, and stored for 2 to 4 days in a −80° freezer. They were then cut into 8- to 10-μm-thick sections with a cryostat (Jung Frigocut 2800 N, Leica Inc, Wetzlar, Germany), transferred to a glass slide, and imaged immediately with a digital camera (RT Color, 1X HRD 100-NIK, Diagnostic Instruments, Inc) mounted on a light microscope (Leica type 301-371.010, Leica Inc) at ×25 magnification. Myolaminae coursing in the direction noted from the frozen specimen were observed (sheets), and over a 1-minute period, gaps between the cleavage planes appeared between the myolaminae. Using image processing software, we measured 5 β angles between sheet orientations (Xs) and X_3 normal to the endocardial face over the length of the specimen. Mean β was used to characterize the sheet angle at each transmural depth.

Strain Analysis

Transmural Cardiac Strains

Transmural bead placement enabled the assessment of myocardial deformations of LV wall in the lateral equatorial and anterior basal regions. For each beat, the reference (undeformed) state was taken at end diastole for that beat, and the ensuing positions of the beads for that beat were defined by displacement from their positions at end diastole as characterized by a continuous polynomial position field with quadratic dependence in X_3 and bilinear dependence in X_1 and X_2 using least-squares minimization. For each time sample analyzed, X_3 (radial axis) was defined normal to the epicardial tangent plane created by the 3 epicardial surface beads, with origin (O) at the centroid of these 3 epicardial beads (Figure 1): X_2 (longitudinal axis) was defined at the intersection of the epicardial plane with a plane containing X_3 and a line (long axis) λ_1 (anterior wall) and λ_2 (lateral wall) from the apex marker through the origin (long-axis λ_1 aligns within 8° of the long axis defined by Harrington et al[9]); X_1 (circumferential axis) was defined normal to X_2 and X_3. In cardiac coordinates (X_1, X_2, X_3), the 3 normal strain components measure local myocardial stretch or shortening along the circumferential (E_{11}), longitudinal (E_{22}), and radial (E_{33}) cardiac axes. The 3 shear strains (E_{12}, E_{13}, and E_{23}) represent angle changes between pairs of the originally orthogonal coordinate axes. Strains were interpolated along the centroid of the bead columns at 1% increments of wall depth from the epicardium to the most subendocardial bead. Cardiac normal and shear strains were calculated at 20%, 50%, and 80% depths from the epicardium, with end diastole as the reference configuration and end systole as the deformed configuration for both the anterior and lateral LV wall. More detailed strain analysis has been previously provided.[6,8]

Transmural Fiber-Sheet Strains

In each heart, at each transmural depth, cardiac finite strains (ie, relative to X_1, X_2, and X_3; Figure 1) were transformed into sheet strains at that depth oriented along the fiber, sheet, and sheet-normal axes by application of the fiber (α) and sheet (β) angle measurements in that heart at that depth as follows:

(1)

$$\begin{bmatrix} E_{ff} & E_{fs} & E_{fn} \\ E_{fs} & E_{ss} & E_{sn} \\ E_{fn} & E_{sn} & E_{nn} \end{bmatrix} = \begin{bmatrix} \cos\alpha & \sin\alpha & 0 \\ -\sin\alpha\sin\beta & \cos\alpha\sin\beta & \cos\beta \\ \sin\alpha\cos\beta & -\cos\alpha\cos\beta & \sin\beta \end{bmatrix} \begin{bmatrix} E_{11} & E_{12} & E_{13} \\ E_{12} & E_{22} & E_{23} \\ E_{13} & E_{23} & E_{33} \end{bmatrix} \begin{bmatrix} \cos\alpha & -\sin\alpha\sin\beta & \sin\alpha\cos\beta \\ \sin\alpha & \cos\alpha\sin\beta & -\cos\alpha\cos\beta \\ 0 & \cos\beta & \sin\beta \end{bmatrix}$$

Subsequently, fiber-sheet strains calculated included shortening or stretch along the fiber (E_{ff}), sheet (E_{ss}), and sheet-normal (E_{nn}) directions and 3 shear strains (E_{fn}, E_{fs}, E_{sn}). Next, the contributions of sheet strains to radial thickening (E_{33} strain) were calculated as follows: $E_{33}=EssCos^2\beta+EnnSin^2\beta+2EsnSin\beta Cos\beta$.[1,7]

Statistical Analysis

Data were initially investigated to check for normality. Nonnormal data were transformed with a log transformation before further statistical analysis. All data were compared by use of repeated-measures ANOVA (SigmaStat 3.11, SPSS, Inc, Chicago, Ill). Values of $P<0.05$ were considered statistically significant. Data are reported as mean±SD unless otherwise stated.

The authors had full access to and take full responsibility for the integrity of the data. All authors have read and agree to the manuscript as written.

Results

Table 1 shows group mean anterior basal and lateral equatorial LV transmural fiber angles (α) and sheet angles (β) measured at 20%, 50%, and 80% wall depth from the epicardium. Fiber angles varied linearly with depth and are identical at both regions. Sheet angles exhibited pleated sheet behavior with alternating signs between 20%, 50%, and 80% depths with a roughly mirror image in the 2 LV regions.

Downloaded from circ.ahajournals.org at STANFORD UNIV MEDICAL CENTER on January 27, 2010

Table 2. Transmural Systolic Fiber-Sheet Strains in the Anterobasal and Lateral Equatorial Region at 3 Different LV Wall Depths

	Subepicardium		Midwall		Subendocardium	
	Anterior	Lateral	Anterior	Lateral	Anterior	Lateral
E_{ff}	−0.08±0.07	−0.08±0.04	−0.11±0.09	−0.11±0.05	−0.10±0.05	−0.10±0.08
E_{ss}	0.00±0.04	0.11±0.07	0.22±0.12	0.09±0.06*	−0.06±0.12	−0.04±0.20
E_{nn}	0.16±0.15	0.03±0.06	0.02±0.12	0.08±0.10	0.45±0.40	0.17±0.09*
E_{fs}	−0.03±0.05	−0.01±0.07	−0.03±0.04	0.02±0.03	0.00±0.05	0.10±0.05*
E_{fn}	0.03±0.09	0.01±0.02	−0.03±0.04	−0.07±0.05	−0.06±0.10	0.04±0.05
E_{sn}	−0.14±0.07	0.05±0.03*	0.21±0.12	−0.12±0.06*	−0.19±0.23	0.20±0.15

Group mean±SD data from 9 hearts. E_{ff} indicates fiber strain; E_{ss}, sheet strain; E_{nn}, strain normal to laminae; E_{fs}, fiber-sheet shear; E_{fn}, fiber-normal shear; and E_{sn}, sheet-normal shear.

*$P<0.05$, lateral versus anterior fiber-sheet absolute strain values at the same wall depth. All data between the anterior and lateral LV wall at different levels were compared using repeated-measures ANOVA.

These findings are consistent with those in other hearts from our previous study.[9]

Systolic fiber-sheet strains in both LV regions are summarized in Table 2. E_{ff} was uniformly negative (fiber shortening) and identical in both regions at each transmural depth (Table 2 and Figure 2). Subepicardial and midwall sheet-normal shear (E_{sn}) and subendocardial fiber-sheet shear (E_{fs}) differed significantly between the regions in the anterior and lateral LV walls. Anterior wall subendocardial sheet thickening (E_{nn}) also was significantly greater than that of the lateral LV wall. Midwall sheet extension (E_{ss}) in the anterior wall was double that of the lateral wall.

Table 3 summarizes the transmural components of systolic wall thickening. At each depth, radial wall thickening of the anterior basal wall was significantly greater than that of the lateral equatorial wall (Figure 3). Epicardial and midwall sheet shear (E_{sn}) wall thickening contribution in the anterior wall was 2 times greater than that in the lateral wall (Table 3 and Figure 4). Moreover, the epicardial and endocardial anterior basal sheet thickening (E_{nn}) contributions to wall thickening were >2 times that in the lateral wall.

Figure 4 illustrates the group mean data summing the systolic wall thickening sheet components in the lateral and anterior LV regions. In the lateral LV wall, sheet shear (E_{sn}) was always an important component of systolic wall thickening at all transmural depths (38% in the epicardium, 55% in the midwall, and 60% in the endocardium). Sheet thickening (E_{nn}) was a major wall thickening component in the endocardium (40%) and sheet extension (E_{ss}) in the epicardium (46%).

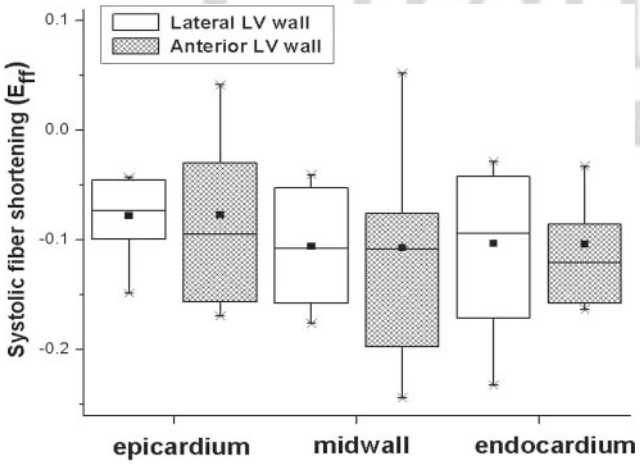

Figure 2. Box plot of systolic fiber shortening (E_{ff}) in lateral equatorial (open bars) and anterior basal (hatched bars) LV regions. Data from 9 hearts. Abscissa is wall depth. No statistically significant differences were noted. All data between the anterior and lateral LV walls at different levels were compared by use of repeated-measures ANOVA. Each box plot displays the smallest value (lowest point on vertical whisker), 25th percentile (bottom of box), median (horizontal line in box), group mean (square black symbol in the box), 75th percentile (top of box), and largest value (highest point on vertical whisker).

Table 3. Transmural Components of Systolic Wall Thickening in Lateral Equatorial and Anterobasal Regions

	Anterior Wall	Lateral Wall
Subepicardium		
E_{2033}	0.25±0.15	0.13±0.03*
E_{20ssc}	0.00±0.02	0.06±0.04
E_{20nnc}	0.12±0.11	0.02±0.04*
E_{20snc}	0.13±0.06	0.05±0.03*
Midwall		
E_{5033}	0.34±0.17	0.20±0.12*
E_{50ssc}	0.12±0.08	0.06±0.05
E_{50nnc}	0.02±0.07	0.03±0.04
E_{50snc}	0.20±0.12	0.11±0.06*
Subendocardium		
E_{8033}	0.47±0.30	0.30±0.24*
E_{80ssc}	−0.02±0.06	0.00±0.08
E_{80nnc}	0.31±0.30	0.12±0.09*
E_{80snc}	0.19±0.23	0.18±0.15

Group mean±SD data from 9 hearts.

E_{2033}, E_{5033}, and E_{8033} indicate systolic radial strain at 20%, 50%, and 80% wall depth from epicardium. E_{20ssc}, E_{50ssc}, and E_{80ssc}, SS component of systolic radial strain at 20%, 50%, and 80% wall depth. E_{20nnc}, E_{50nnc}, and E_{80nnc}, NN component of systolic radial strain at 20%, 50%, and 80% wall depth; and E_{20snc}, E_{50snc}, and E_{80snc}, SN component of systolic radial strain at 20%, 50%, and 80% wall depth.

*$P<0.05$ from repeated-measures ANOVA of lateral LV wall data vs anterior LV wall data.

Downloaded from circ.ahajournals.org at STANFORD UNIV MEDICAL CENTER on January 27, 2010

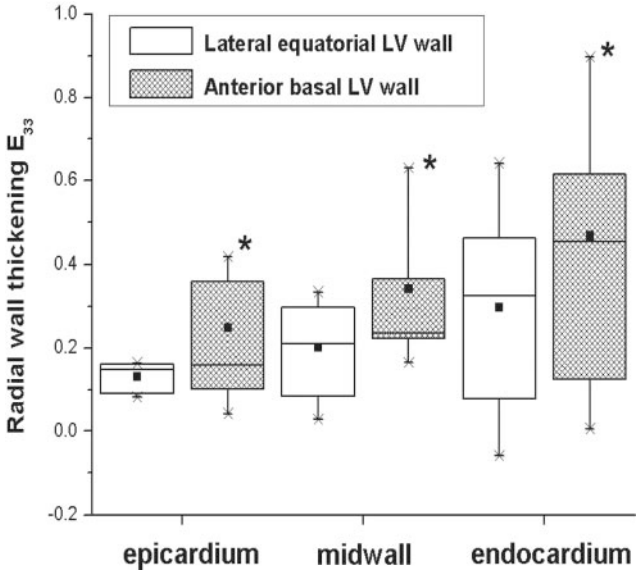

Figure 3. Box plot of radial systolic wall thickening (E_{33}) in the lateral equatorial (open boxes) and anterior basal (hatched boxes) LV walls. Data from 9 hearts. Abscissa is wall depth. Each box plot displays the smallest value (lowest point on vertical whisker), 25th percentile (bottom of box), median (horizontal line in box), group mean (square black symbol in the box), 75th percentile (top of box), and largest value (highest point on vertical whisker). *$P<0.05$ from repeated-measures ANOVA between anterior and lateral E_{33} at each depth.

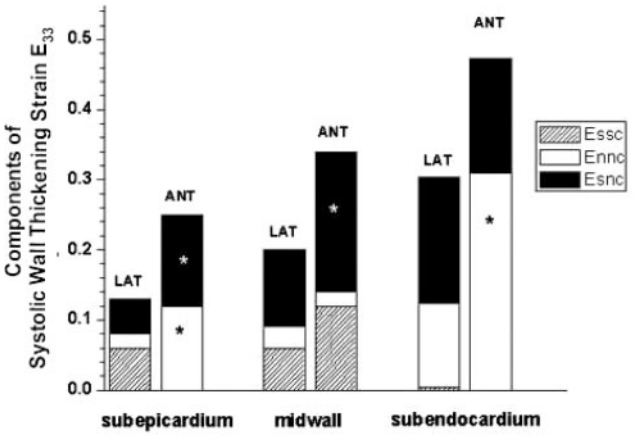

Figure 4. Components of systolic wall thickening in lateral basal and anterior equatorial LV wall. Group mean data (n=9) from Table 3. Ordinate is systolic strain (end diastole is the reference state; end systole is the deformed state); abscissa is wall depth. Each pair of bars displays data at the lateral (LAT) and anterior (ANT) wall. Total height of each bar is the transmural systolic wall thickening strain (E_{33}). Sheet components of E_{33} (derived from the following equation: $E_{33}=E_{ss}Cos^2\beta+E_{nn}Sin^2\beta+2E_{sn}Sin\beta Cos\beta$) are bar heights for sheet extension (E_{ssc}; hatched), sheet thickening (E_{nnc}; open), and sheet-normal shear (E_{snc}; solid). *$P<0.05$ from repeated-measures ANOVA between anterior and lateral walls at the same wall depth.

In the anterior LV wall, sheet shear (E_{sn}) remained a significant component of systolic wall thickening at all transmural depths (52% in the epicardium, 58% in the midwall, and 40% in the endocardium). Sheet thickening (E_{nn}) was a major wall thickening component in the epicardium (48%) and endocardium (66%), with sheet extension (E_{ss}) more important in the midwall (35%).

Discussion

The principal findings of this study were the following: (1) Group mean radial wall thickening in the anterobasal region was 1.6 to 1.9 times that of the lateral equatorial region; (2) group mean systolic fiber shortening was identical at each transmural depth in each region; (3) fundamental heterogeneity exists in regional contributions of laminar mechanisms for amplifying fiber shortening to systolic wall thickening; and (4) fiber orientations are similar between these regions, but sheet orientations differ widely. Thus, fiber shortening drives systolic wall thickening, but sheet dynamics, orientations, and probably intercellular connections are of great importance to systolic wall thickening.

Systolic LV radial wall thickening (for a review, see Reference 8) is an important component of normal LV function because of its substantial contribution to stroke volume and its sensitivity to hypoperfusion and altered metabolism.[11–13] Present clinical approaches to evaluate regional ventricular function are based mainly on wall thickening. Although myocardial fiber contraction provides the basic mechanics for regional myocardial wall thickening, 15% fiber shortening along the long axis leads to only an 8% increase in myocyte diameter. Yet, 40% radial LV wall thickening and 60% ejection fraction are typically observed.[1,2] Myocardial fibers have been shown to be organized into laminar "sheets" ≈3 to 4 cells thick that are interconnected by an extensive extracellular matrix that provides various degrees of myocyte coupling within each sheet and between adjacent sheets. It was first suggested that reorientation of transmural sheets of fibers could provide a basis for LV wall mechanics during relaxation and contraction.[5] Subsequently, it was demonstrated that reorientation of longitudinal-radial cleavage planes owing to transverse shear could account for the majority of end-systolic wall thickening strain.[3] Costa et al[1] then showed that systolic sheet extension and sheet-normal shear also could be primary determinants of systolic wall thickening (Figure 5).

Placement of the transmural bead sets allows measurement of transmural cardiac strains along the longitudinal, circumferential, and radial axes. By performing direct microstructural measurements[7,9] in the region of the bead sets, we can transform these cardiac strains into fiber and sheet strains, and these transforms can be used to characterize wall thickening components through the LV wall.

Transmural radial wall thickening in the anterobasal wall was found to be considerably greater than that of the lateral equatorial wall. However, systolic fiber shortening was identical at each transmural depth in both regions. To more fully comprehend this phenomenon, we examined the fiber and sheet strain contributions to systolic wall thickening.

In these ovine hearts, systolic fiber shortening (E_{ff}) was 8% to 11% (Table 2) and did not exhibit a transmural gradient, which is consistent with previous predictions and observations.[1,14] Interestingly, as seen in previous canine[1] and human[15] studies, sheet sheet-normal shear E_{sn} in these ovine hearts greatly exceeded fiber sheet-normal shear E_{fn} (Table 2). This preference for sheet sliding relative to one another

Downloaded from circ.ahajournals.org at STANFORD UNIV MEDICAL CENTER on January 27, 2010

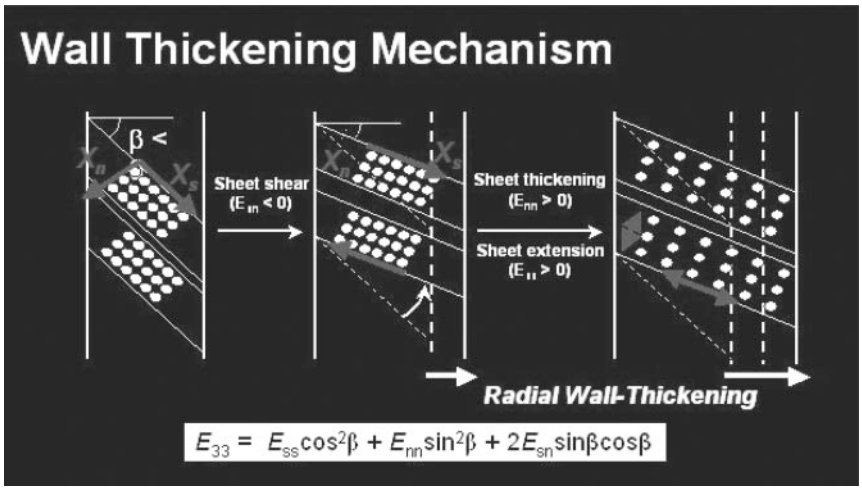

Figure 5. Components of systolic LV wall thickening. A schematic model relating sheet geometry to systolic wall thickening. Fibers are grouped into sheets 3 to 4 cells thick. Sheet shear (E_{sn}) measures the sliding of adjacent sheets relative to one another, with the resulting sheet reorientation in the radial direction producing wall thickening. The radial components of sheet extension (E_{ss}) and thickening (E_{nn}) also produce wall thickening.

along the sheet direction, rather than between fibers within the sheets, may reflect a tighter coupling of myocytes by extensive collagen networks within the sheets and a looser coupling between adjacent sheets.

In the lateral LV wall, similar to our previous findings,[7] the present study showed that sheet shear (E_{sn}) is always an important component of systolic wall thickening at all transmural depths. Furthermore, sheet thickening (E_{nn}) is dominant in the endocardium, although sheet extension (E_{ss}) contributes importantly in the epicardium.

In the anterior basal LV wall, similar to the findings of Costa et al[1] in the same region, sheet shear remains a dominant component of systolic wall thickening at all transmural depths. E_{nn} is positive (sheet thickening) and contributes significantly to wall thickening in both the epicardium and endocardium. This finding, however, differs from that reported by Costa et al,[1] who found that E_{nn} was small and negative (sheet thinning) at the anterior basal site. We believe sheet thickening is probably more likely during systole, whereas sheet thinning is more difficult to explain and may require cellular interdigitation. It is possible that the thinning they observed could result in part from the small β measured by their indirect histological approach in canine hearts;[1] we measured much larger β values with our direct histological approach applied to the same region in ovine hearts. Moreover, a different species (canine versus ovine) was used in their study, which also may contribute to the differences in sheet orientation and strains between the 2 studies.

Using diffusion tensor MRI to obtain sheet structure and strain rate, Dou et al[15] reported midsystolic sheet dynamics at the equatorial LV level in normal human hearts and found substantial contributions of E_{ss}, E_{sn}, and E_{nn} to E_{33} in the lateral and anterior walls. Similar to our findings, they demonstrated that a major contribution to radial thickening was associated with sheet-related strains and that the 3 components of fiber-related strains contributed less to radial thickening. Their study, however, differed from the present study by reporting average contributions over the entire transmural thickness at each LV site owing to resolution limitations. The present study suggests that considerable transmural sheet geometry and strains remain to be revealed by magnetic resonance imaging as its spatial resolution increases.

With these data describing the heterogeneity in sheet contribution to systolic wall thickening, the next question was, "What accounts for these differences in the 2 regions?" To answer this question, the structural differences, ie, fiber and sheet orientations, were explored.

The present study, applying a direct measurement approach to the ovine anterior basal and lateral equatorial LV walls, demonstrated that fiber angles varied linearly with depth (Table 1), as seen in previous studies.[7,9] This helical myofiber orientation is relatively preserved among different species,[1,16–19] ranging from approximately $-60°$ to $60°$ from epicardium to endocardium, ie, from a left-handed helix in the epicardium to a right-handed helix in the endocardium with circumferential fibers at midwall. More important, in the present study, the transmural distribution of fiber angles was found to be similar in both the anterior and lateral LV regions. Thus, both fiber orientation and fiber shortening cannot explain the regional differences in systolic wall thickening.

A dramatic difference in the sheet angles in these 2 regions was found, as illustrated in Figure 6 and Table 1, with 1 being the mirror image of the other across the LV wall in the epicardium, midwall, and endocardium. This is consistent with our previous study[7,9] in which sheet angles fell into 2 distinct families: β^- and β^+. In the lateral equatorial wall, near the epicardium, β belonged to the β^+ family; near the midwall, to the β^- family; and near the endocardium, again to the β^+ family. In the anterior basal wall, the reverse trend was observed: Near the epicardium, β belonged to the β^- family; near the midwall, to the β^+ family; and near the endocardium, again to the β^- family. Figure 6 presents a conceptual schematic model depicting 1 way that the results observed in these 3 regions can be synthesized into a more global picture of the cardiac microstructure.

Described previously,[9] this accordion-like laminar distribution allows alternating shear displacements to occur within the wall that reduces the shear displacements required of the epicardium relative to the endocardium. With this mechanism, shear deformations can be roughly the same throughout the wall, but the direction of sheet sliding alternates.

Although distribution of α for these hearts (Table 1) was virtually indistinguishable from that observed in the canine basal anterior wall,[1] distributions of β were distinctly differ-

Downloaded from circ.ahajournals.org at STANFORD UNIV MEDICAL CENTER on January 27, 2010

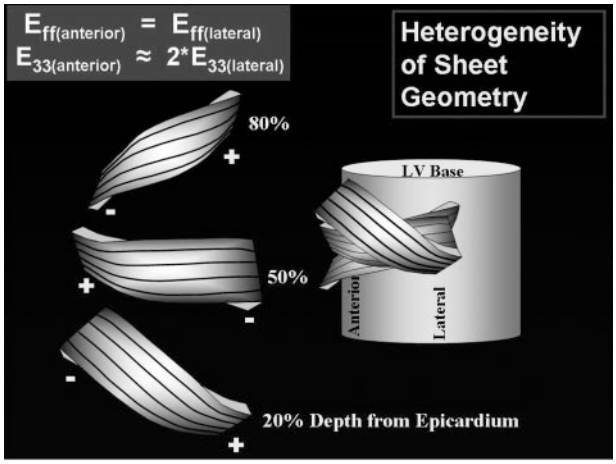

Figure 6. Fiber and sheet orientations. A model synthesizing fiber and sheet data from anterior and lateral equatorial regions of the heart. The illustration on the left represent sheets at 20%, 50%, and 80% wall depth from the epicardium. Black lines on the surface of the sheets represent measured α qualitatively, with negative α values near the epicardium, values of 0° at midwall, and positive α values near the epicardium. Left margins of the sheets represent data from the anterior wall, with sheets belonging to the negative β family at 20%, to the positive β family at 50%, and to the negative β family at 80% wall depth. Right region of the sheets represent data from the lateral region, with sheets belonging to the positive β family at 20%, to the negative β family at 50%, and to the positive β family at 80% wall depth from the epicardium.

ent. Costa et al,[1] using indirect measurements, reported mean basal anterior wall β values of 0° at 20% depth to −20° at 50% and 80% depths from the epicardium. We found, by direct measurement, much greater magnitudes of β in a pleated-accordion pattern, ranging from a mean of −55° at 20% depth to 43° at 50% depth and then back to −52° at 80% depth (Table 1).

Chen et al,[20] using diffusion tensor magnetic resonance imaging with isolated rat hearts, found that sheet angles changed from 36° at end diastole to 20° at end systole, reflecting a change in sheet orientation during ventricular contraction. Their observations provide further evidence that fiber and sheet geometry alterations during systole provide a fundamental mechanism for regional systolic LV wall thickening.

Rohmer et al,[21] using diffusion-tensor magnetic resonance imaging, found that fiber angles vary smoothly across the LV wall from epicardium (negative angles) to endocardium (positive angles) in human hearts, similar to our findings and previous canine and ovine studies.[7,9] They also attempted to identify the sheet model, which is broadly similar to that proposed by Legrice et al[4] and Costa et al[1] in which the sheet architecture is complex, with sheet orientations depending on myocardial location.

In summary, these data demonstrate fundamentally different regional contributions of laminar mechanisms for amplifying fiber shortening to systolic wall thickening. Systolic fiber shortening was identical at each transmural depth in both the anterior and lateral LV sites, yet systolic wall thickening of the anterior site was 60% to 90% greater than that of the lateral site. Fiber shortening drives systolic wall thickening, but sheet dynamics and sheet geometry are of great importance to systolic wall thickening. In other words, myocyte contraction contributes to radial wall thickening and ventricular ejection both by myocyte shortening and by the related secondary induction of changes in fiber and sheet organization. This mechanism depends critically on the orientation of the myocytes and their interaction with the extracellular matrix throughout the ventricular wall during systole.

The complexity of this mechanism of wall thickening suggests that abnormalities in either the contractile unit (fiber and sheet) or the infrastructure (extracellular matrix) can dramatically affect wall thickening. The characterization of the baseline 3-dimensional myocardial architecture and dynamics is important because collagen degradation can be brought about by disease states[22] and altered baseline myocyte infrastructure may be a key mechanism in ventricular dysfunction.[17,23]

Normal cardiac microstructure and systolic strains are tightly coupled, and deviations could result in apoptosis and matrix remodeling.[24–29] Recent studies indicate that developed ventricular wall stress is very sensitive to changes in fiber and sheet structure over the cardiac cycle.[30–32] Thus, it is conceivable that evaluation of preclinical abnormalities of ventricular function could be improved by incorporating quantitative data on fiber and sheet structure in systole. Furthermore, characterization of such structural changes in diseased hearts may facilitate the investigation of the mechanisms of structural and functional adaptations in the ventricular remodeling process.

The enhanced understanding of the myocardial fibrous and laminar architecture, transmural LV strains, and LV wall mechanics could contribute significantly to the design of better surgical remodeling procedures to restore normal ventricular strain patterns in patients with cardiomyopathy. Sheet geometry, strains, and intercellular matrix coupling are crucial for LV wall thickening and dynamics. The present study suggests that attempts to implant healthy contractile cells into diseased hearts or to surgically manipulate cardiac geometry must take into account not only the contraction of cardiac cells but, of equal importance, their orientation and transmural coupling, which may be specific to each ventricular region.

Study Limitations

Considerable caution is warranted before extrapolation of these results to the human heart.

Fiber angle (α) measurements are relatively straightforward and reproducible, but sheet angle (β) measurements are more difficult. As discussed, it is quite possible that there are major species and regional differences in transmural sheet angle measurements (although this may only strengthen the concept that variations in the macrostructure of the wall are important in determining wall thickening). Multiple β populations are found at different wall depths, particularly in the subendocardium. It is not appropriate to average these populations because they often are of opposite sign and could average, inappropriately, to zero. Our approach in the present study, as in other previous studies,[1,7,9,33] was to measure and

Downloaded from circ.ahajournals.org at STANFORD UNIV MEDICAL CENTER on January 27, 2010

use the dominant β population in our analysis, assuming that the predominant orientation would have the major effect on LV wall thickening. But, future work is needed to understand the functional importance of regions with multiple β populations.

Although myocardial deformations were directly measured in this study, fiber and sheet strains were calculated from a structural model of the LV wall. The spatial resolution of the present study was insufficient to allow inferences regarding individual cell or sheet shape changes during systole, although measurement of such changes will be an important, but very difficult, future goal. It should also be emphasized that collagen content and geometry or elasticity of the intracellular matrix were not measured in this study.

Our observations are limited only to the lateral equatorial and anterior basal ovine LV walls. However, it should be emphasized that the findings of this study show, despite identical regional systolic fiber shortening, that regional sheet dynamics and orientations different importantly within the left ventricle and are very important to systolic wall thickening and LV function. The results of the present study encourage a thorough and systematic study of the entire LV. Placement of transmural bead sets is invasive. Magnetic resonance imaging will ultimately be the best method for this type of study. It is noninvasive and will allow assessment of the entire LV rather than a few specific regions. However, the current spatial resolution of magnetic resonance imaging is not sufficient to make the required measurements directly. Most magnetic resonance imaging studies have reported average strain contributions over the entire transmural thickness at each LV site or used model assumptions for each LV wall depth.

Acknowledgments

We appreciate the superb technical assistance provided by Mary K. Zasio, BA; Maggie Brophy, AS; and Mark Grisedale, DVM.

Sources of Funding

Supported by grants HL-29589 and HL-67025 from the National Heart, Lung and Blood Institute. Drs Cheng and Nguyen were Carl and Leah McConnell Cardiovascular Surgical Research Fellows and were recipients of the Thoracic Society Foundation Research Fellowship Award.

Disclosures

None.

References

1. Costa KD, Takayama Y, McCulloch AD, Covell JW. Laminar fiber architecture and three-dimensional systolic mechanics in canine ventricular myocardium. *Am J Physiol*. 1999;276:H595–H607.
2. Sonnenblick EH, Ross J Jr, Covell JW, Spotnitz HM, Spiro D. The ultrastructure of the heart in systole and diastole: changes in sarcomere length. *Circ Res*. 1967;21:423–431.
3. LeGrice IJ, Takayama Y, Covell JW. Transverse shear along myocardial cleavage planes provides a mechanism for normal systolic wall thickening. *Circ Res*. 1995;77:182–193.
4. LeGrice IJ, Smaill BH, Chai LZ, Edgar SG, Gavin JB, Hunter PJ. Laminar structure of the heart: ventricular myocyte arrangement and connective tissue architecture in the dog. *Am J Physiol*. 1995;269:H571–H582.
5. Spotnitz HM, Spotnitz WD, Cottrell TS, Spiro D, Sonnenblick EH. Cellular basis for volume related wall thickness changes in the rat left ventricle. *J Mol Cell Cardiol*. 1974;6:317–331.
6. Cheng A, Langer F, Nguyen TC, Malinowski M, Ennis DB, Daughters GT, Ingels NB Jr, Miller DC. Transmural left ventricular shear strain alterations adjacent to and remote from infarcted myocardium. *J Heart Valve Dis*. 2006;15:209–218.
7. Cheng A, Langer F, Rodriguez F, Criscione JC, Daughters GT, Miller DC, Ingels NB Jr. Transmural sheet strains in the lateral wall of the ovine left ventricle. *Am J Physiol Heart Circ Physiol*. 2005;289:H1234–H1241.
8. Cheng A, Langer F, Rodriguez F, Criscione JC, Daughters GT, Miller DC, Ingels NB Jr. Transmural cardiac strains in the lateral wall of the ovine left ventricle. *Am J Physiol Heart Circ Physiol*. 2005;288:H1546–H1556.
9. Harrington KB, Rodriguez F, Cheng A, Langer F, Ashikaga H, Daughters GT, Criscione JC, Ingels NB, Miller DC. Direct measurement of transmural laminar architecture in the anterolateral wall of the ovine left ventricle: new implications for wall thickening mechanics. *Am J Physiol Heart Circ Physiol*. 2005;288:H1324–H1330.
10. Rodriguez F, Langer F, Harrington KB, Cheng A, Daughters GT, Criscione JC, Ingels NB, Miller DC. Alterations in transmural strains adjacent to ischemic myocardium during acute midcircumflex occlusion. *J Thorac Cardiovasc Surg*. 2005;129:791–803.
11. Gould KL, Kennedy JW, Frimer M, Pollack GH, Dodge HT. Analysis of wall dynamics and directional components of left ventricular contraction in man. *Am J Cardiol*. 1976;38:322–331.
12. Dumesnil JG, Shoucri RM. Quantitative relationships between left ventricular ejection and wall thickening and geometry. *J Appl Physiol*. 1991;70:48–54.
13. Gallagher KP, Gerren RA, Stirling MC, Choy M, Dysko RC, McManimon SP, Dunham WR. The distribution of functional impairment across the lateral border of acutely ischemic myocardium. *Circ Res*. 1986;58:570–583.
14. Arts T, Reneman RS, Veenstra PC. A model of the mechanics of the left ventricle. *Ann Biomed Eng*. 1979;7:299–318.
15. Dou J, Tseng WY, Reese TG, Wedeen VJ. Combined diffusion and strain MRI reveals structure and function of human myocardial laminar sheets in vivo. *Magn Reson Med*. 2003;50:107–113.
16. Takayama Y, Costa KD, Covell JW. Contribution of laminar myofiber architecture to load-dependent changes in mechanics of LV myocardium. *Am J Physiol Heart Circ Physiol*. 2002;282:H1510–H1520.
17. Weis SM, Emery JL, Becker KD, McBride DJ Jr, Omens JH, McCulloch AD. Myocardial mechanics and collagen structure in the osteogenesis imperfecta murine (OIM). *Circ Res*. 200;87:663–669.
18. Knisley SB, Baynham TC. Line stimulation parallel to myofibers enhances regional uniformity of transmembrane voltage changes in rabbit hearts. *Circ Res*. 1997;81:229–241.
19. Greenbaum RA, Ho SY, Gibson DG, Becker AE, Anderson RH. Left ventricular fibre architecture in man. *Br Heart J*. 1981;45:248–263.
20. Chen J, Liu W, Zhang H, Lacy L, Yang X, Song SK, Wickline SA, Yu X. Regional ventricular wall thickening reflects changes in cardiac fiber and sheet structure during contraction: quantification with diffusion tensor MRI. *Am J Physiol Heart Circ Physiol*. 2005;289:H1898–H1907.
21. Rohmer D, Siteck A, Gullberg GT. Reconstruction and visualization of fiber and laminar structures in the normal human heart from ex vivo diffuse tensor magnetic resonance imaging (DTMRI) data. *Invest Radiol*. 2007;42:777–789.
22. Weber KT, Sun Y, Tyagi SC, Cleutjens JP. Collagen network of the myocardium: function, structural remodeling and regulatory mechanisms. *J Mol Cell Cardiol*. 1994;26:279–292.
23. Chen J, Song SK, Liu W, McLean M, Allen JS, Tan J, Wickline SA, Yu X. Remodeling of cardiac fiber structure after infarction in rats quantified with diffusion tensor MRI. *Am J Physiol Heart Circ Physiol*. 2003;285:H946–H954.
24. Kang PM, Izumo S. Apoptosis and heart failure: a critical review of the literature. *Circ Res*. 200;86:1107–1113.
25. Saraste A, Pulkki K, Kallajoki M, Henriksen K, Parvinen M, Voipio-Pulkki LM. Apoptosis in human acute myocardial infarction. *Circulation*. 1997;95:320–323.
26. Olivetti G, Abbi R, Quaini F, Kajstura J, Cheng W, Nitahara JA, Quaini E, Di Loreto C, Beltrami CA, Krajewski S, Reed JC, Anversa P. Apoptosis in the failing human heart. *N Engl J Med*. 1997;336:1131–1141.
27. Tyagi SC, Lewis K, Pikes D, Marcello A, Mujumdar VS, Smiley LM, Moore CK. Stretch-induced membrane type matrix metalloproteinase and tissue plasminogen activator in cardiac fibroblast cells. *J Cell Physiol*. 1998;176:374–382.
28. Wilson EM, Moainie SL, Baskin JM, Lowry AS, Deschamps AM, Mukherjee R, Guy TS, John-Sutton MG, Gorman JH III, Edmunds LH Jr,

Downloaded from circ.ahajournals.org at STANFORD UNIV MEDICAL CENTER on January 27, 2010

Gorman RC, Spinale FG. Region- and type-specific induction of matrix metalloproteinases in post-myocardial infarction remodeling. *Circulation*. 2003;107:2857–2863.
29. Bowen FW, Jones SC, Narula N, John Sutton MG, Plappert T, Edmunds LH Jr, Dixon IM. Restraining acute infarct expansion decreases collagenase activity in borderzone myocardium. *Ann Thorac Surg*. 2001;72:1950–1956.
30. Rijcken J, Bovendeerd PH, Schoofs AJ, van Campen DH, Arts T. Optimization of cardiac fiber orientation for homogeneous fiber strain during ejection. *Ann Biomed Eng*. 1999;27:289–297.
31. Rijcken J, Arts T, Bovendeerd P, Schoofs B, van Campen D. Optimization of left ventricular fibre orientation of the normal heart for homogeneous sarcomere length during ejection. *Eur J Morphol*. 1996;34:39–46.
32. Bovendeerd PH, Arts T, Huyghe JM, van Campen DH, Reneman RS. Dependence of local left ventricular wall mechanics on myocardial fiber orientation: a model study. *J Biomech*. 1992;25:1129–1140.
33. Ashikaga H, Criscione JC, Omens JH, Covell JW, Ingels NB Jr. Transmural left ventricular mechanics underlying torsional recoil during relaxation. *Am J Physiol Heart Circ Physiol*. 2004;286:H640–H647.

CLINICAL PERSPECTIVE

Left ventricular (LV) wall thickening is a significant contributor to stroke volume. Although myocardial fiber contraction provides the cellular basis for regional myocardial wall thickening, 15% fiber shortening leads to only an 8% increase in myocyte diameter, which cannot explain the observed >40% radial LV wall thickening and >60% ejection fraction. Myocardial fibers have been shown to be grouped into laminar "sheets" 3 to 4 cells thick that are interconnected by an extensive extracellular matrix. This study demonstrates fundamentally different regional contributions of laminar mechanisms for amplifying fiber shortening to systolic wall thickening. Systolic fiber shortening was identical at each transmural depth in both the anterior and lateral LV sites, but systolic wall thickening of the anterior site was much greater than that of the lateral site. This implies that sheet geometry and dynamics and the exact nature of their coupling by the extracellular matrix are of great importance to systolic wall thickening. The complexity of this mechanism of wall thickening suggests that abnormalities in either the contractile unit (fiber and sheet) or the infrastructure (extracellular matrix) can dramatically affect wall thickening. The characterization of the baseline 3-dimensional myocardial architecture and dynamics is important because collagen degradation can be brought about by disease states, and altered baseline myocyte infrastructure may be a key mechanism in ventricular dysfunction. Enhanced understanding of myocardial fibrous and laminar architecture coupling to transmural LV strains and LV wall mechanics could contribute significantly to the design of better surgical remodeling procedures to restore normal ventricular strain patterns in patients with cardiomyopathy. Furthermore, attempts to implant healthy contractile cells or tissue-engineered constructs into diseased hearts or to surgically manipulate cardiac geometry must take into account not only the contraction of cardiac cells but, of equal importance, their orientation and transmural coupling, which may be specific to each ventricular region and transmural depth.

American Heart Association
Fighting Heart Disease and Stroke
Circulation
Journal of the American Heart Association

Downloaded from circ.ahajournals.org at STANFORD UNIV MEDICAL CENTER on January 27, 2010